2-D TIME EVOLUTION OF T_e DURING A SAWTOOTH CRASH BASED ON FAST ECE MEASUREMENTS ON TFTR

G. Kuo-Petravic

Plasma Physics Laboratory, Princeton University

Princeton, NJ 08543 USA

PPPL--2556

DE89 006859

ABSTRACT

Electron cyclotron emission measurements taken at 20 locations in the horizontal mid-plane during a sawtooth crash have been analysed based on the assumption of fast rigid rotation of the plasma. Due to this fast rotation($\approx 100\mu sec$), which remains fairly constant throughout the sawtooth crash, we have been able to make time-to-space reconstructions of half the poloidal plane using points which are separated in time by not more than $40\mu sec$. The existence of a temperature flattening in the precursor phase, which we interpret as an m=1 temperature island, is clearly demonstrated, and its location and width agree well with local emissivity measurements from soft x-ray tomography viewing the same poloidal plane [G.Kuo-Petravic PPPL-2555, 1988]. The rotating temperature island in the precursor phase, the outward movement of the region of high T_e during the crash phase, and the shape of T_e distribution after the crash during the successor phase have all been documented in a time sequence of color contours.

1. INTRODUCTION

Recently, measurements have been made of electron cyclotron emission (ECE) from TFTR during a sawtooth crash phase. The experimental setup [1] is shown in Figs. 1 and 2. Emission from the horizontal midplane is focussed by a reflector and sent to a grating spectrometer. From 20 channels of the spectrometer we obtain information on local electron temperatures, T_e, at intervals of approximately 5.5 cm along a major radius both inside and outside the magnetic axis. Owing to the presence of harmonics, we cannot measure beyond 1/2 of the way in minor radius, that is, around 40 cm. Viewing the same poloidal plane horizontally is an array of soft x-ray detectors used for tomographic analysis [2]. We, therefore, have a means of cross-correlating two independent sets of measurements and data processing methods for the same sawtooth crash. This is invaluable for validating both the tomographic method with Fourier-transformed variables and the time-to-space reconstruction method based on the rigid rotation of the plasma. In this paper we shall discuss two reconstruction methods which assume that the fast rigid rotation of the plasma brings T_e information for the entire poloidal plane into the field of view. The observed flattening of the temperature profile in the precursor phase, which we interpret as an m=1 island, correlates well with the tomography results, giving strong proof of the validity of the ECE reconstruction method, at least in the precursor phase.

In order to make the analysis easier, a discharge (shot no. 30904) was chosen which had as fast a rotation as possible compared to the sawtooth crash time. The parameters of the discharge were: plasma current I_p=1.7 MA, average electron density $\bar{N}_e$ = 3.8 x10^{19} / m^3, major radius R =2.46 m, minor radius a = 0.81 m, and neutral beam power $P_B = 19.9 MW$.

2. METHOD OF ANALYSIS

The 20 channels of ECE data were digitized at 100 kHz with 8K of memory per channel. In Figs. 3a, 3b, and 3c we show raw data from three channels at the following radii: a) R=234 cm, b) R=239 cm and, c) R=259 cm, respectively. These are typical of the three distinct regions important in sawtooth instability, namely, regions where $q < 1$, $q \approx 1$, and $q > 1$ respectively, q being the safety factor. Figures 3d, 3e, and 3f are enlargements of Figs. 3a, 3b, and 3c in the vicinity of the sawtooth crash. It is necessary to locate the centers of the flux surfaces in the midplane because we assume that they are also the centers of rotation. The extent of the Shafranov shifts may be found by displaying T_e averaged over a rotation period versus the minor radius, r, using any assumed value of R_{major} (Fig. 4). A spline fit to these data shows up the symmetry points which are defined as the midpoints in radius for a given T_e. Since we are interested mainly in the region of plasma from the magnetic axis to around the q=1 surface, that is, $0 < r < 30$ cm, we shall assume one midpoint, which is also the center of rotation, for all the flux surfaces. The effects of neglecting the differences in Shafranov shifts and shear in angular velocity for the flux surfaces contribute to not more than 1 cm of uncertainty in the reconstruction process.

Figure 5, which corresponds to a channel near the q=1 surface, shows the data points and the time interval analysed. First of all, we observe that the repetition rate remains approximately constant throughout this range of time at $\approx 100\mu$sec. The first three periods comprise the end of a long sequence of oscillations which exhibit extreme regularity both in frequency and amplitude and which have been in existence since the start of the digitizer 50 msec back. This is termed the precursor phase of the sawtooth instability. The next

oscillation shows a much enhanced amplitude due to the outward movement of the region of high T_e in the crash phase. Finally, we analyse three oscillations of the successor phase which are again more regular but smaller in amplitude.

Because of the fast rotation, we can think of the plasma as being advected to the positions of the 20 channels every Δt seconds(in our case the sampling time Δt= 10μsec). In Fig. 6 we show how it is possible to convert this sequence in time into a spatial distribution in the given poloidal plane. Figure 6a is a schematic diagram showing a sequence of signals at constant radius both outside($P_1, P_2, ...P_{10}$) and inside($M_1, M_2, ...M_{10}$) the magnetic axis plotted against real time t. At time $t = t_6$ the signal at the location of the outside channel in the midplane is, of course, t_6, while the signal at the same location at time $t = t_7$ may be interpreted as the signal at poloidal location $\theta = \pi/5$ at time t_6 assuming clockwise rotation. That is, the signal at $t = t_n$, P_n, can be interpreted as the signal at $\theta = (n - N - 1)\pi/N$, where 2N=total number of points per rotation period. In our case, N=5 and n=7, ...10 for the outer channels for reconstruction at $t = t_6$. Similarly, we can map the sequence of signals in time in the inside channels onto the region below the midplane. For a clockwise rotation the inside signals are lagging in phase by π from the outside signals. Therefore, a sequence of signals $P_6, P_7, ...P_{10}, M_6, M_7, ...M_{10}$ maps out the entire poloidal distribution of T_e at time t_6 (unweighted method). For the distribution at $t = t_7$ we need only advance in time(Fig. 6a) by Δt: the sequence is then $P_7, P_8, ...P_{11}.M_7, M_8, ...M_{11}$. It is clear that this reconstruction uses information $(N - 1)\Delta t$ away from the real time of the distribution to which it contributes. While this is perfectly acceptable in the precursor phase, it is less so in the crash phase, since the crash happens over $\approx$ 50 - 100 μsec, which is just about the rotation

period, $2N\Delta t$. This time is to be compared with the maximum real time difference between signals on a given frame of reconstruction, which is $(N-1)\Delta t = 40\mu sec$ in our present setup. It may be argued [3] that it is desirable to give more weight to the data points closer in time to the time of the reconstructed distribution, t_n, and de-emphasize points further away in time. This weighted method involves using additional (N-1) points ahead of t_n both on the outside ($P_{n-1}, P_{n-2}, ...P_{n-N+1}$) and the inside ($M_{n-1}, M_{n-2}, ...M_{n-N+1}$). We use the weighted average of two signals, one from either side, separated in real time by a half-period $N\Delta t$. This is shown in Fig.6a as dashed diagonal lines joining the inside data to the outside. The signal at $\theta = (n-N-1)\pi/N$ for a reconstructed distribution at t_n is now given by $((2N-m+1)P_m + (m-N-1)M_{m-N})/N$, where m=n,n+1,...n+N-1, for $\theta < \pi$, and similarly for $\pi < \theta < 2\pi$. Since we have now involved points over a full rotation period rather than half a period in the unweighted method, we are back to the same conclusion that the weighted method also should work very well for the precursor phase and less well for the crash phase.

3. RESULTS

Both methods of reconstruction, weighted and unweighted, have been implemented and applied to the time interval marked by arrows A and B in Fig. 5. In Figs. 7 and 8 we show the weighted reconstructions of T_e both as contours and 3-D plots at selected times marked by arrows (1) to (8) in Fig. 5. Similarly those for unweighted reconstruction are shown in Figs. 9 and 10. In our particular shot (no. 30904), where the rotation period is 100 μsec,

if the T_e of an element of plasma at location $\theta = 4\pi/5$ at time t changes appreciably on the scale of the reconstruction time $\approx 4\Delta t$, then a large error may occur. This is because by the time this element reaches the location of the detector channel at t=t+4Δt, a different value of T_e would be registered. Since this situation probably pertains to the crash phase, it may be more accurate to use the unweighted method for this phase with the understanding that regions $\pi/2 < \theta < \pi$ and $3\pi/2 < \theta < 2\pi$ are not as accurate as the remaining regions, where reconstruction is derived from signals closer in time. Comparison of the two methods as represented by Figs. 7 to 10 does not reveal any qualitative differences for the precursor and successor phases, as would be expected. However, the crash phase, as given by the unweighted method, is sharper while the weighted method produces smoother profiles, a result of averaging over twice the time interval.

The above procedures apply to periods of rotation that are integral multiples of Δt, which generally do not occur. We have extended the unweighted method to allow for varying periods of rotation. First, the rotation periods are measured by subtracting from the signal of Fig. 5 a smooth signal obtained by time averaging over one rotation period. Once the periods have been determined, the time sequence of signals can then be laid out on the poloidal plane according to their phases.

ACKNOWLEDGMENTS

I am very grateful to Drs. K.M. McGuire and A. Cavallo for guidance thoroughout the course of this work.

This work supported by U.S. DOE Contract No. DE-AC02-76-CHO-3073.

Note : An animated sequence of T_e profiles in contours of 255 colors was made on a Macintosh II with the aid of IMAGETOOL [4]. Anyone wishing to view a videotape of this reconstruction may contact the author.

REFERENCES

[1] A. CAVALLO, T. CUTLER, and M. McCARTHY, Rev. Sci. Instum. (1988) to be published.

[2] G. KUO-PETRAVIC, Princeton Plasma Physics Laboratory Report No. PPPL-2555 (1988).

[3] R. GOLDSTON, Private Communication. (1988).

[4] T. REDMAN and C.C. LAM, IMAGETOOL, Nat. Lab. for Supercomputer Applications, Univ. of Illinois, Champaign-Urbana, Illinois (1987).

FIGURE CAPTIONS

Figure 1 Schematic diagram of a TFTR poloidal plane showing the positions of the 20 ECE channels.

Figure 2 Schematic diagram of the experimental setup for ECE measurements.

Figure 3 A sawtooth crash on TFTR showing electron temperature at different major radii.

(a) T_e at R=234 cm from time 4.773 to 4.781 sec. The dashed lines mark the time interval of Fig. 3d.

(b) T_e at R=239 cm from time 4.773 to 4.781 sec.

(c) T_e at R=259 cm from time 4.773 to 4.781 sec.

(d) T_e at R=234 cm from time 4.7770 to 4.7778 sec.

(e) T_e at R=239 cm from time 4.7770 to 4.7778 sec.

(f) T_e at R=259 cm from time 4.7770 to 4.7778 sec.

Figure 4 T_e averaged over one rotation period versus minor radius r.

Figure 5 Expanded view of the sawtooth crash at R=239 cm. Reconstruction was performed for the time interval A to B. The arrows (1) to (8) indicate the times corresponding to the graphs of Figures 7 to 10.

Figure 6

(a) Schematic diagram of signals, P, from an outside channel and, M, from an inside channel at the same radius as a function of real time t. The heavy line with arrows joins data points which become contiguous in space in the poloidal reconstruction of T_e.

(b) The reconstructed poloidal distribution of T_e for $t = t_6$ using the unweighted method.

(c) The reconstructed poloidal distribution of T_e for $t = t_6$ using the weighted method .

Figure 7 Contours of constant T_e for the weighted method for the times indicated by arrows (1) to (8) in Fig. 5.

Figure 8 3-D plots of T_e for the weighted method for the times indicated by arrows (1) to (8) in Fig. 5.

Figues 9 Contours of constant T_e for the unweighted method for the times indicated by arrows (1) to (8) in Fig. 5.

Figure 10 3-D plots of T_e for the unweighted method for the times indicated by arrows (1) to (8) in Fig. 5.

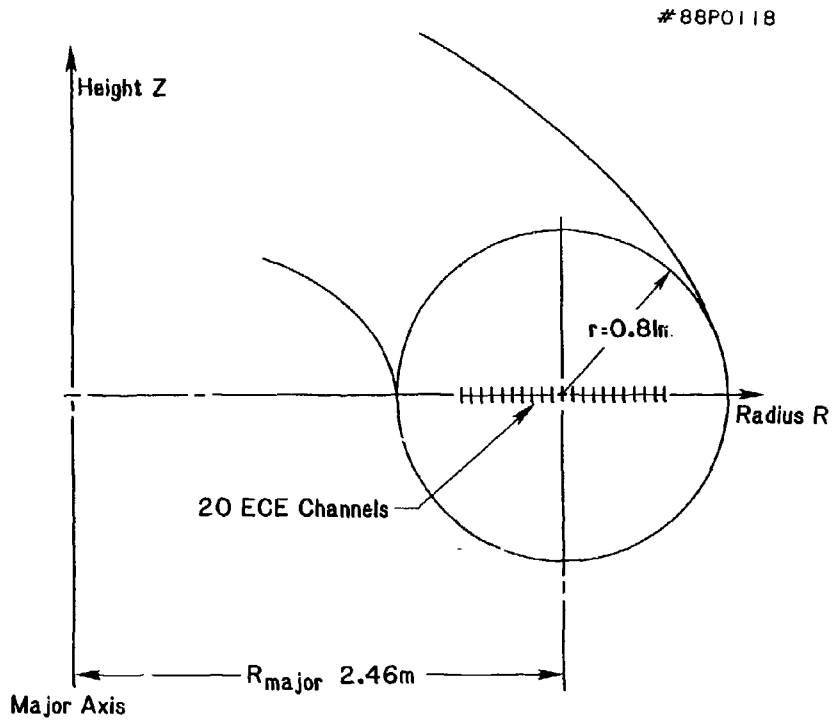
#88P0118
Height Z
r=0.81m
Radius R
20 ECE Channels
R major 2.46m
Major Axis

Fig. 1

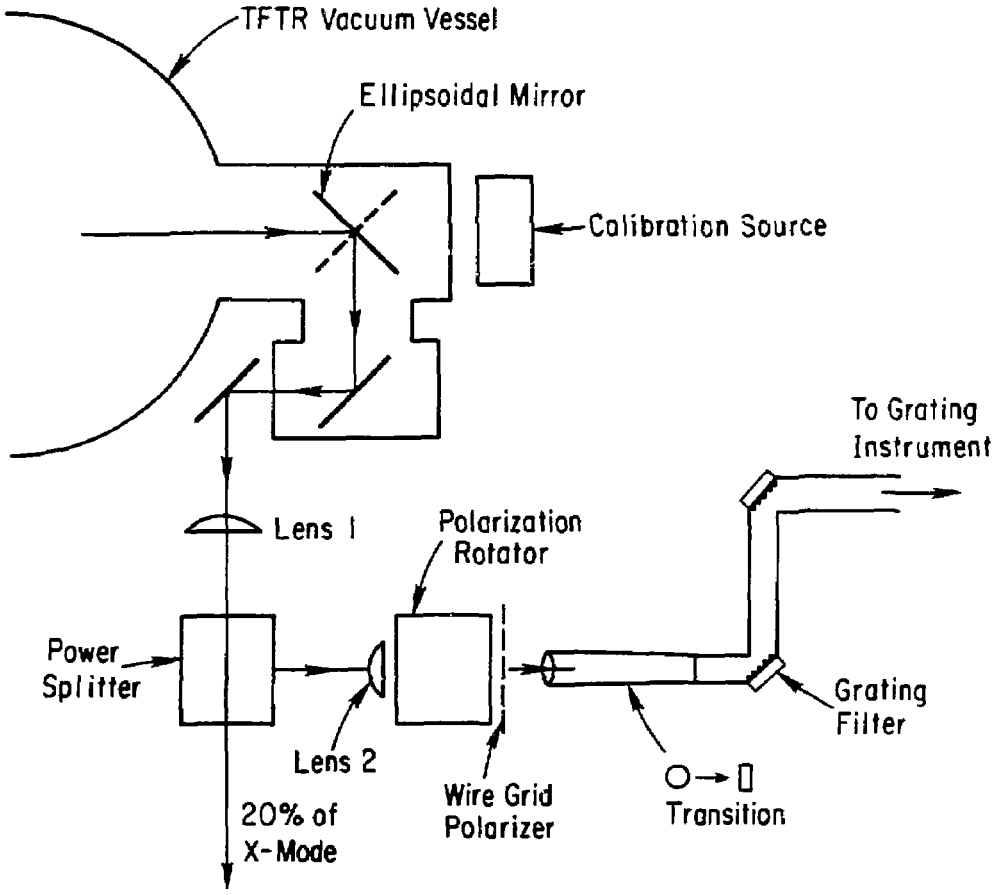
TFTR Vacuum Vessel
Ellipsoidal Mirror
Calibration Source
To Grating
Instrument
Lens 1
Polarization
Rotator
Power
Splitter
Grating
Filter
Lens 2
Wire Grid
Polarizer
Transition
20% of
X-Mode

Fig. 2

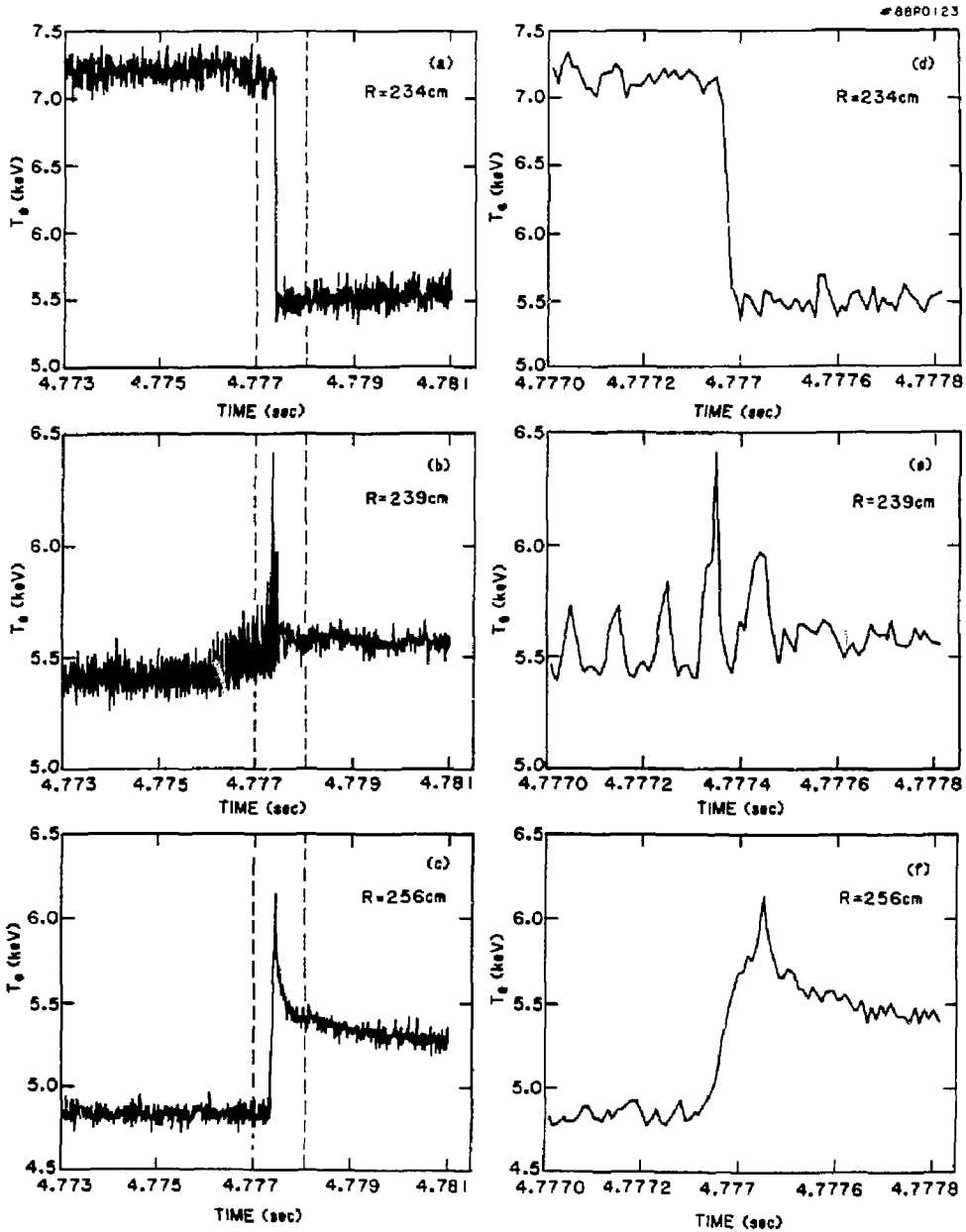
#88P0123
(a)
R=234cm
(d)
R=234cm
(b)
R=239cm
(e)
R=239cm
(c)
R=256cm
(f)
R=256cm
T_e (keV)
TIME (sec)

Fig. 3

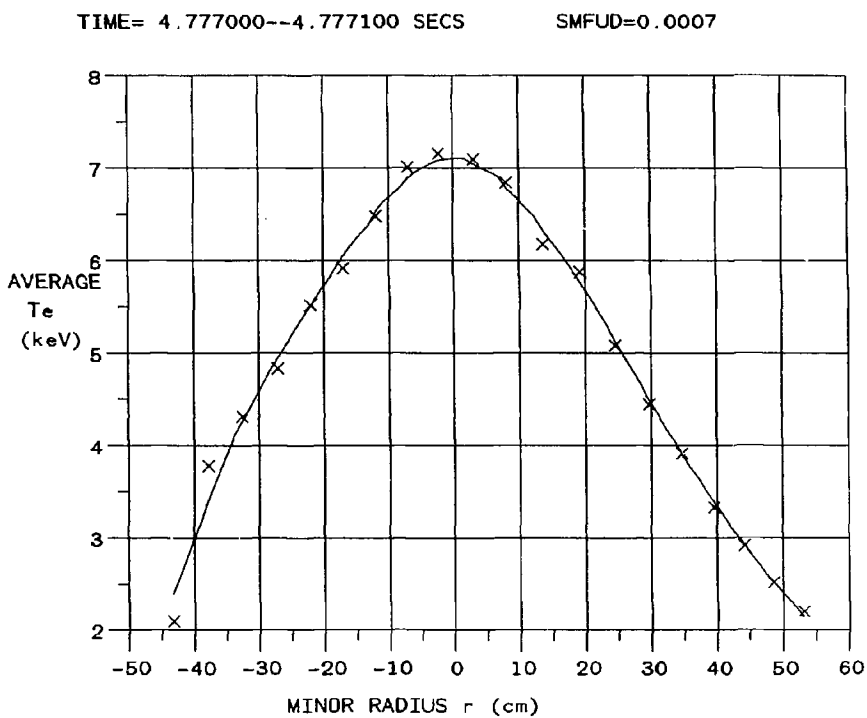
TIME= 4.777000--4.777100 SECS
SMFUD=0.0007
AVERAGE
Te
(keV)
8
7
6
5
4
3
2
-50
-40
-30
-20
-10
0
10
20
30
40
50
60
MINOR RADIUS r (cm)

Fig. 4

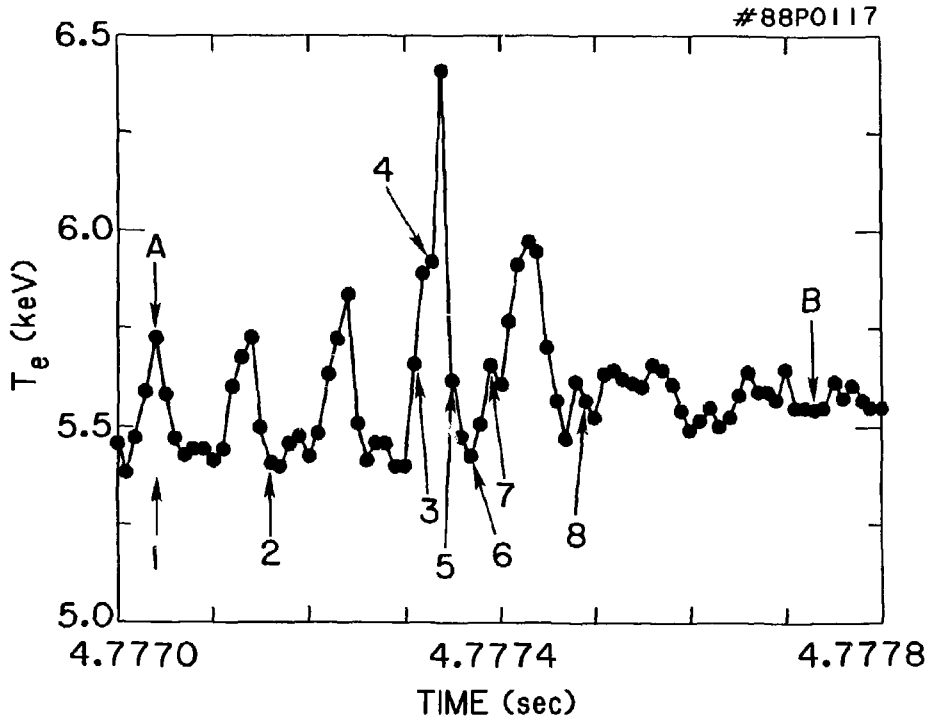
#88P0117
6.5
6.0
5.5
5.0
T_e (keV)
A
B
1
2
3
4
5
6
7
8
4.7770
4.7774
4.7778
TIME (sec)

Fig. 5

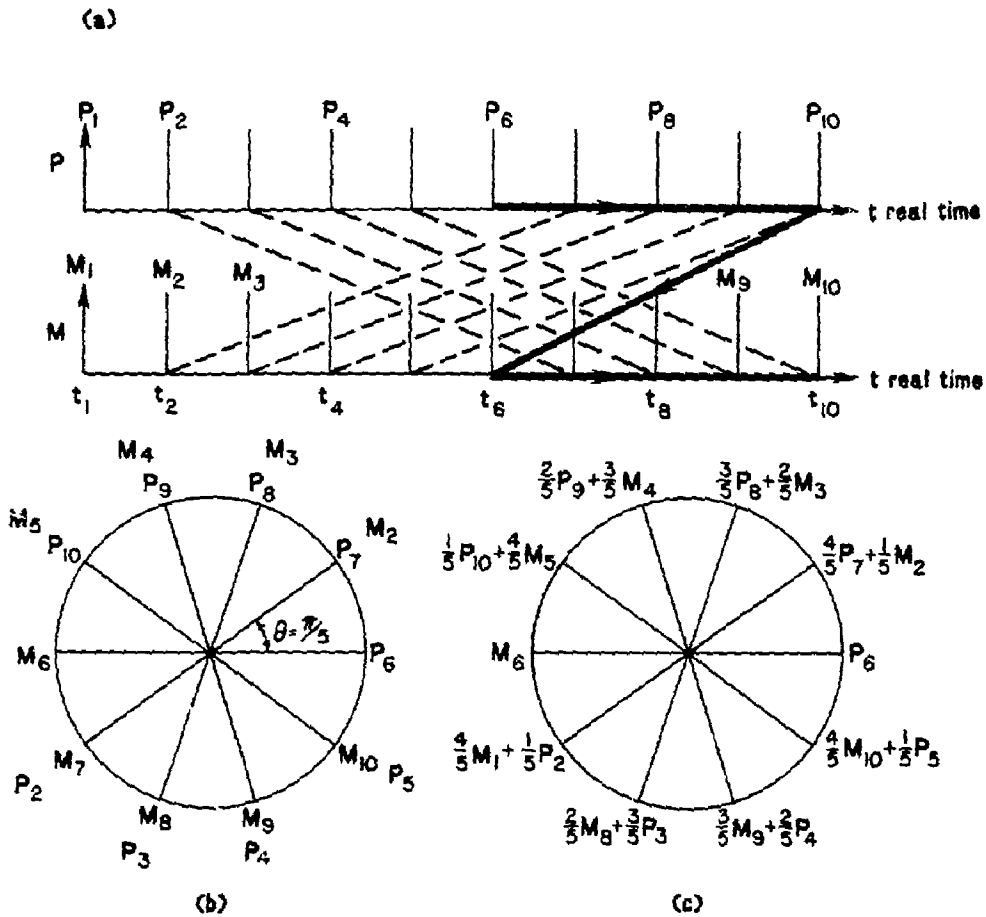

Fig. 6

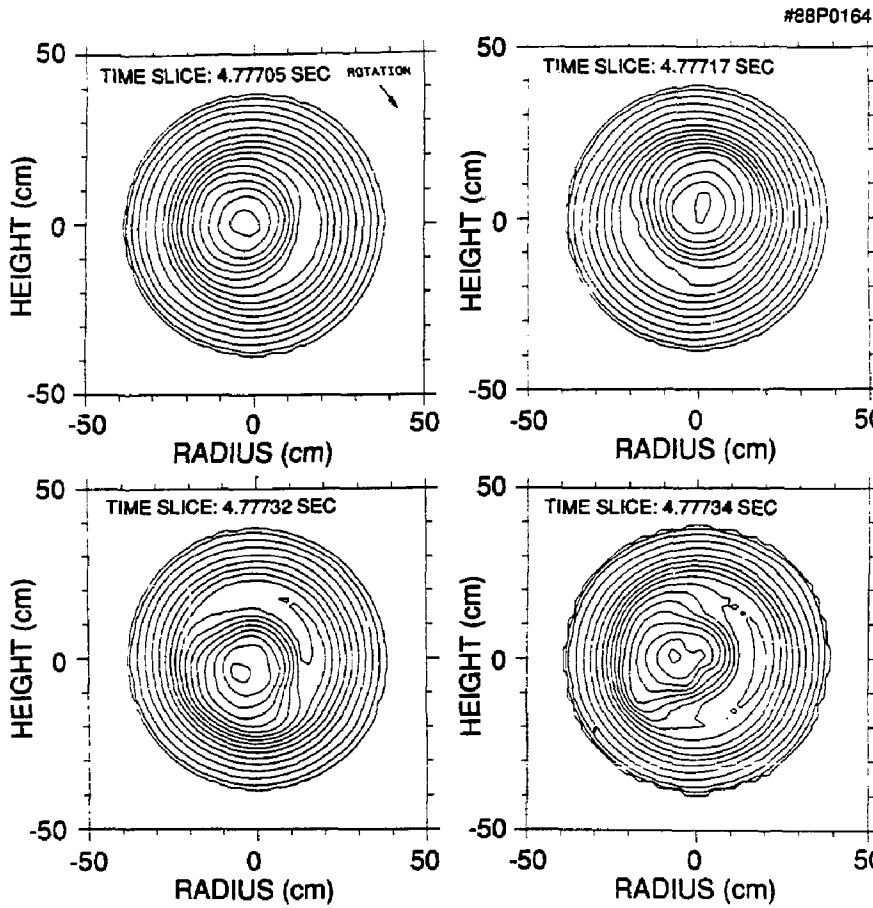
#88P0164
TIME SLICE: 4.77705 SEC
ROTATION
TIME SLICE: 4.77717 SEC
TIME SLICE: 4.77732 SEC
TIME SLICE: 4.77734 SEC
HEIGHT (cm)
RADIUS (cm)
50
0
-50

Fig. 7a

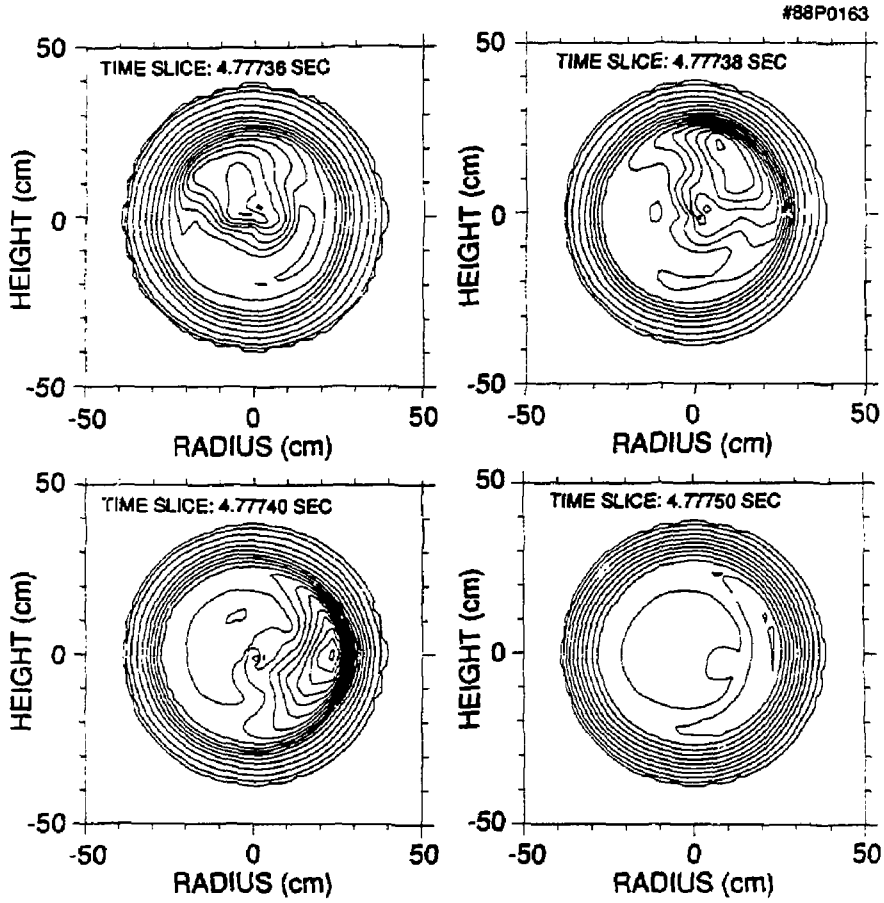
#88P0163
TIME SLICE: 4.77736 SEC
TIME SLICE: 4.77738 SEC
TIME SLICE: 4.77740 SEC
TIME SLICE: 4.77750 SEC
HEIGHT (cm)
RADIUS (cm)
50
0
-50

Fig. 7b

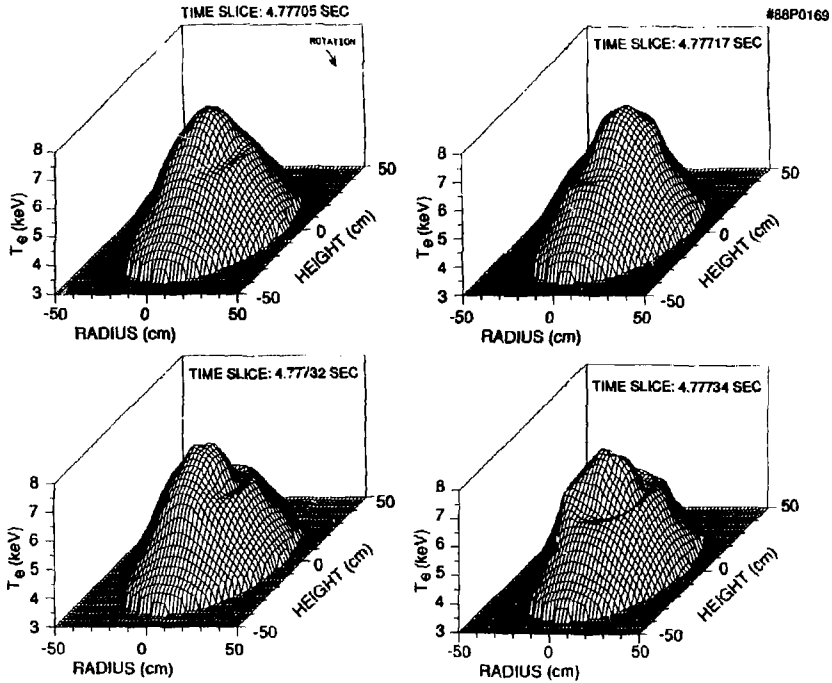
TIME SLICE: 4.77705 SEC
ROTATION
#88P0169
TIME SLICE: 4.77717 SEC
TIME SLICE: 4.77732 SEC
TIME SLICE: 4.77734 SEC
T_e (keV)
RADIUS (cm)
HEIGHT (cm)
-50
0
50
3
4
5
6
7
8

Fig. 8a

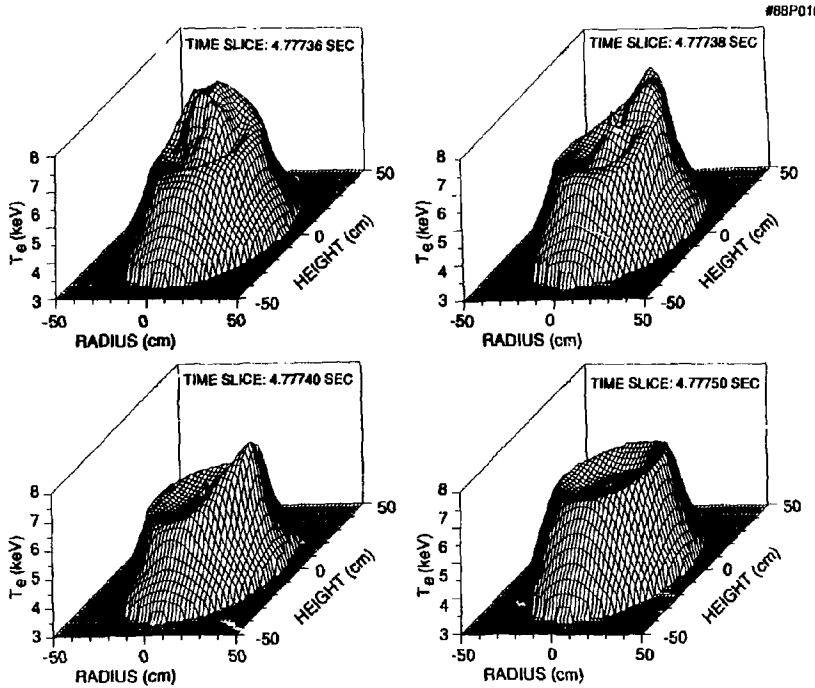
#88P0168
TIME SLICE: 4.77736 SEC
TIME SLICE: 4.77738 SEC
TIME SLICE: 4.77740 SEC
TIME SLICE: 4.77750 SEC
T_e (keV)
RADIUS (cm)
HEIGHT (cm)
8
7
6
5
4
3
-50
0
50

Fig. 8b

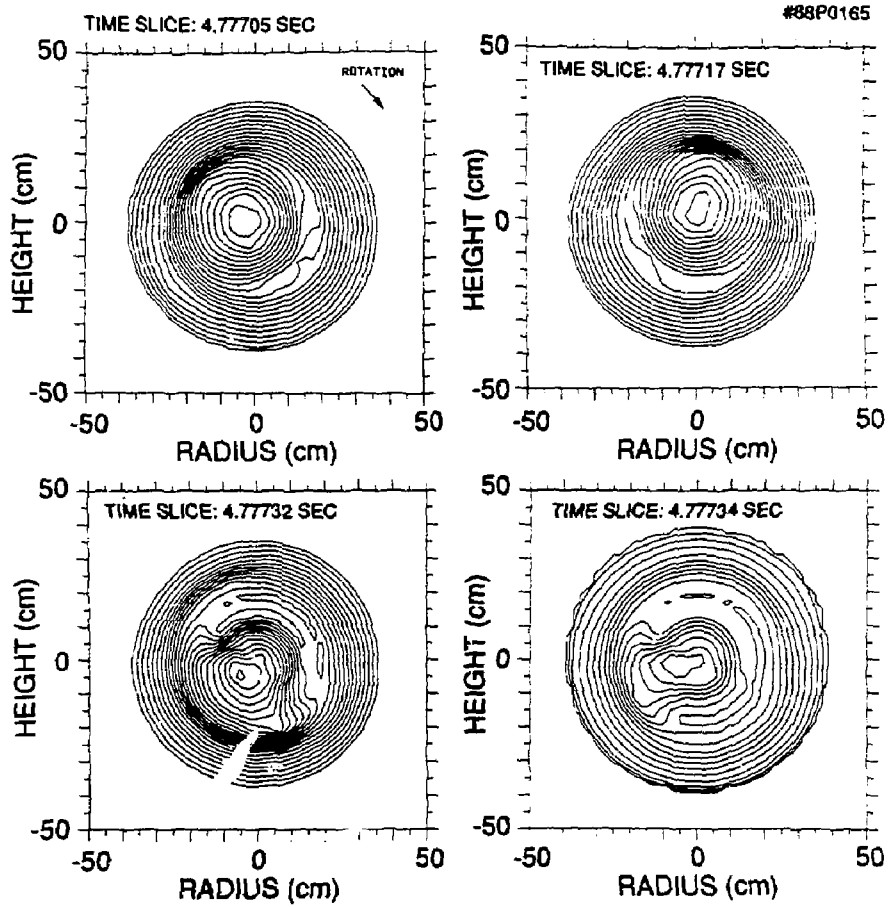
#88P0165
TIME SLICE: 4.77705 SEC
ROTATION
TIME SLICE: 4.77717 SEC
TIME SLICE: 4.77732 SEC
TIME SLICE: 4.77734 SEC
HEIGHT (cm)
RADIUS (cm)
50
0
-50

Fig. 9a

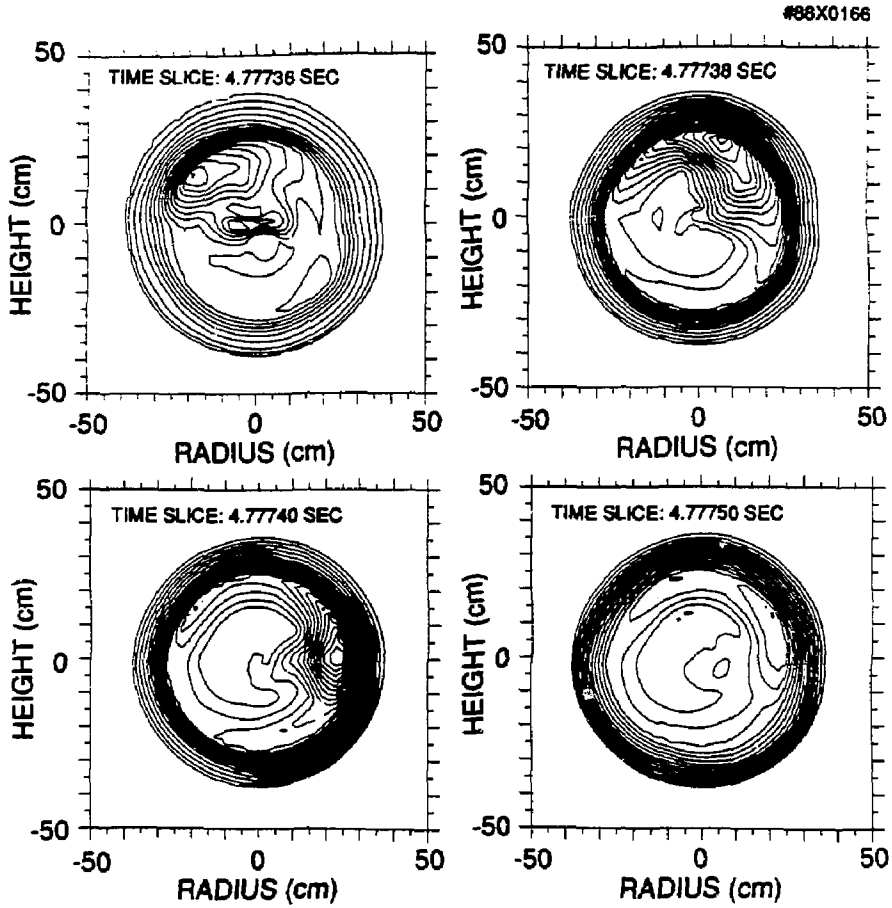
#86X0166
TIME SLICE: 4.77736 SEC
TIME SLICE: 4.77738 SEC
TIME SLICE: 4.77740 SEC
TIME SLICE: 4.77750 SEC
HEIGHT (cm)
RADIUS (cm)
50
0
-50

Fig. 9b

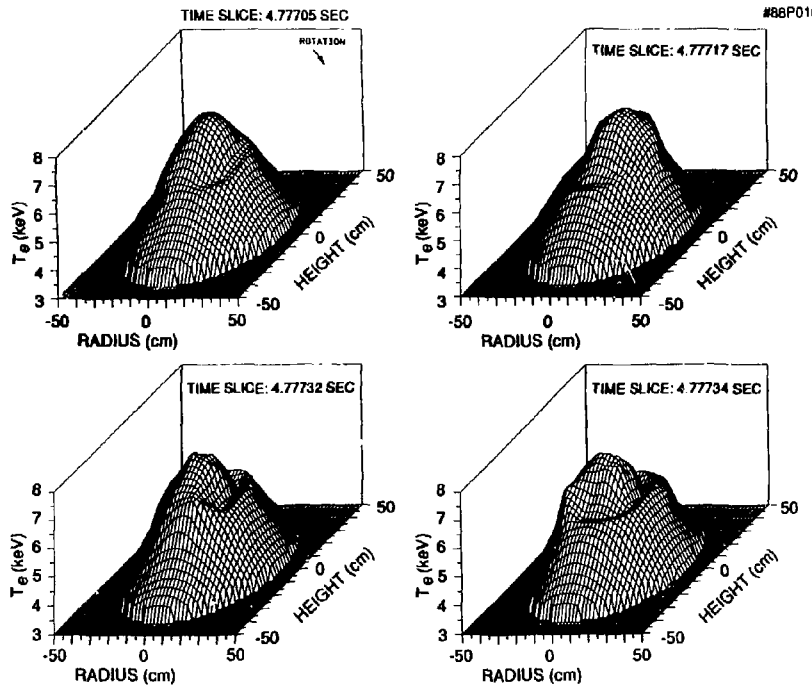
TIME SLICE: 4.77705 SEC
ROTATION
#88P0167
TIME SLICE: 4.77717 SEC
TIME SLICE: 4.77732 SEC
TIME SLICE: 4.77734 SEC
T_e (keV)
RADIUS (cm)
HEIGHT (cm)
-50
0
50
3
4
5
6
7
8

Fig. 10a

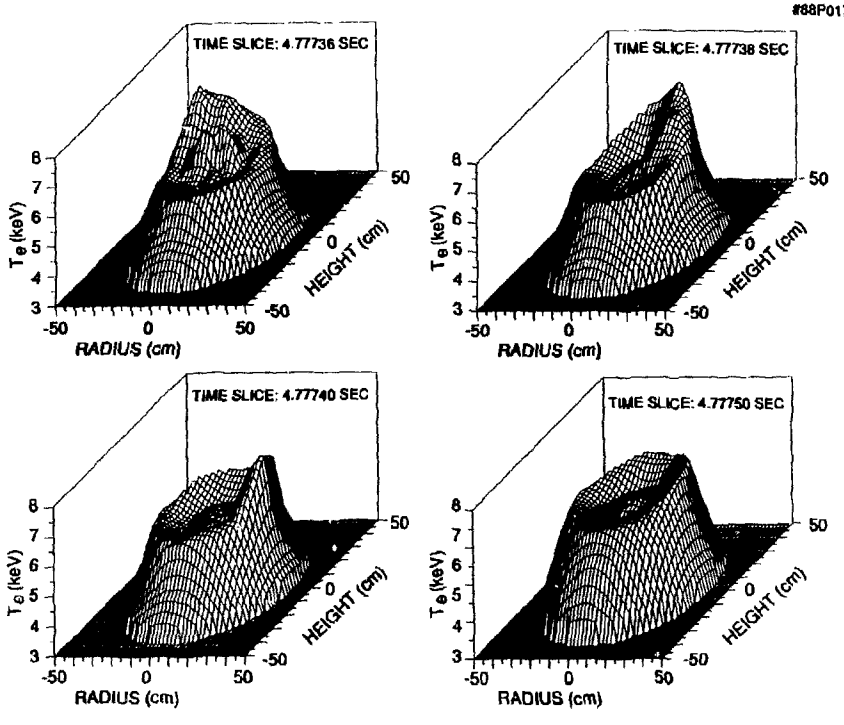
#88P0170
TIME SLICE: 4.77736 SEC
TIME SLICE: 4.77738 SEC
TIME SLICE: 4.77740 SEC
TIME SLICE: 4.77750 SEC
T_e (keV)
RADIUS (cm)
HEIGHT (cm)

Fig. 10b

EXTERNAL DISTRIBUTION IN ADDITION TO UC-20

Dr. Frank J. Paoloni, Univ of Wollongong, AUSTRALIA
Prof. M.H. Brennan, Univ Sydney, AUSTRALIA
Plasma Research Lab., Australian Nat. Univ., AUSTRALIA
Prof. I.R. Jones, Flinders Univ., AUSTRALIA
Prof. F. Cap, Inst Theo Phys, AUSTRIA
Prof. M. Heindler, Institut fur Theoretische Physik, AUSTRIA
M. Goossens, Astronomisch Instituut, BELGIUM
Ecole Royale Militaire, Lab de Phys Plasmas, BELGIUM
Commission-European, Dg-XII Fusion Prog, BELGIUM
Prof. R. Boucique, Laboratorium voor Natuurkunde, BELGIUM
Dr. P.H. Sakanaka, Instituto Fisica, BRAZIL
Instituto De Pesquisas Espaciasi-INPE, BRAZIL
Documents Office, Atomic Energy of Canada Limited, CANADA
Dr. M.P. Bacnynski, MPB Technologies, Inc., CANADA
Dr. H.M. Skarsgard, University of Saskatchewan, CANADA
Dr. H. Barnard, University of British Columbia, CANADA
Prof. J. Teichmann, Univ. of Montreal, CANADA
Prof. S.R. Sreenivasan, University of Calgary, CANADA
Prof. Tudor W. Johnston, INRS-Energie, CANADA
Dr. C.R. James, Univ. of Alberta, CANADA
Dr. Peter Lukac, Komenskeho Univ, CZECHOSLOVAKIA
The Librarian, Culham Laboratory, ENGLAND
The Librarian, Rutherford Appleton Laboratory, ENGLAND
Mrs. S.A. Hutchinson, JET Library, ENGLAND
C. Mouttet, Lab. de Physique des Milieux Ionises, FRANCE
J. Radet, CEN/CADARACHE - Bat 506, FRANCE
Univ. of Ioannina, Library of Physics Dept. GREECE
Dr. Tom Mual, Academy Bibliographic Ser., HONG KONG
Preprint Library, Hungarian Academy of Sciences, HUNGARY
Dr. B. Dasgupta, Saha Inst of Nucl. Phys., INDIA
Dr. P. Kaw, Institute for Plasma Research, INDIA
Dr. Phillip Rosenau, Israel Inst. Tech, ISRAEL
Librarian, Int'l Ctr Theo Phys, ITALY
Prof. G. Rostagni, Univ Di Padova, ITALY
Miss Clelia De Palo, Assoc EURATOM-ENEA, ITALY
Biblioteca, Instituto di Fisica del Plasma, ITALY
Dr. H. Yamato, Toshiba Res & Dev, JAPAN
Prof. I. Kawakami, Atomic Energy Res. Institute, JAPAN
Prof. Kyoji Nishikawa, Univ of Hiroshima, JAPAN
Direc. Dept. Large Tokamak Res. JAERI, JAPAN
Prof. Satoshi Itoh, Kyushu University, JAPAN
Research Info Center, Nagoya University, JAPAN
Prof. S. Tanaka, Kyoto University, JAPAN
Library, Kyoto University, JAPAN
Prof. Nobuyuki Inoue, University of Tokyo, JAPAN
S. Mori, JAERI, JAPAN
Librarian, Korea Advanced Energy Res. Institute, KOREA
Prof. D.I. Choi, Adv. Inst Sci & Tech, KOREA
Prof. B.S. Liley, University of Waikato, NEW ZEALAND
Institute of Plasma Physics, PEOPLE'S REPUBLIC OF CHINA
Librarian, Institute of Phys., PEOPLE'S REPUBLIC OF CHINA
Library, Tsing Hua University, PEOPLE'S REPUBLIC OF CHINA
Z. Li, Southwest Inst. Physics, PEOPLE'S REPUBLIC OF CHINA
Prof. J.A.C. Cabral, Inst Superior Tecnico, PORTUGAL
Dr. Octavian Petrus, AL I CUZA University, ROMANIA
Dr. Johan de Villiers, Fusion Studies, AEC, SO AFRICA
Prof. M.A. Hellberg, University of Natal, SO AFRICA
C.I.E.M.A.T., Fusion Div. Library, SPAIN
Dr. Lennart Stenflo, University of UMEA, SWEDEN
Library, Royal Inst Tech, SWEDEN
Prof. Hans Wilhelmson, Chalmers Univ Tech, SWEDEN
Centre Phys des Plasmas, Ecole Polytech Fed, SWITZERLAND
Bibliotheek, Fom-Inst Voor Plasma-Fysica, THE NETHERLANDS
Dr. D.D. Ryutov, Siberian Acad Sci, USSR
Dr. G.A. Eliseev, Kurchatov Institute, USSR
Dr. V.A. Glukhikh, Inst Electrophysical Apparatus, USSR
Dr. V.T. Tolok, Inst. Phys. Tech, USSR
Dr. L.M. Kovrizhnykh Institute Gen. Physics, USSR
Nuclear Res. Establishment, Julich Ltd., W. GERMANY
Bibliothek, Inst. Fur Plasmaforschung, W. GERMANY
Dr. K. Schindler, Ruhr Universitat Bochum, W. GERMANY
ASDEX Reading Rm, IPP/Max-Planck-Institut fur Plasmaphysik, W. GERMANY
Librarian, Max-Planck Institut, W. GERMANY
Prof. R.K. Janev, Inst Phys, YUGOSLAVIA